Chapter 1

Self-Organised Nanoparticle Assemblies: A Panoply of Patterns

Christopher P. Martin[a,1], Matthew O. Blunt[a,1], Emmanuelle Vaujour[a], Amir Fahmi[b], Anthony D'Aleo[c], Luisa De Cola[d], Fritz Vögtle[e], Philip Moriarty[a,2]

[a] *School of Physics & Astronomy, University of Nottingham, Nottingham NG7 2RD, UK*
[b] *School of Mechanical, Materials, and Manufacturing Engineering, Faculty of Engineering, University of Nottingham, Nottingham NG7 2RD, UK*
[c] *Universiteit van Amsterdam, Nieuwe Achtergracht 166, 1018 WV Amsterdam, The Netherlands*
[d] *Physikalisches Institut, Mendelstrasse 7, D-48149 Münster, Germany*
[e] *Kekulé-Institut für Organische Chemie & Biochemie, Universität Bonn, Gerhard-Domagk-Str. 1, D-53121 Bonn, Germany*

Abstract. An overview of self-organisation in an archetypal nanostructured system—2D nanoparticle assemblies—is given. We first focus on the parallels that may be drawn for pattern formation in nanoscopic, microscopic, and macroscopic systems (spanning, for example, nanoparticle arrays, phase-separated polymers, diatom microskeletons, and binary fluid separation) before discussing the quantification of morphology and topology in nanostructured matter. The question of quantification is of key importance for the development of *programmable* or *directed* assembly and we highlight the central role that image morphometry can play in the software control of matter. The nanostructured systems we describe are, in very many cases, far from their ground state and we show that Monte Carlo simulations (based on the approach pioneered by Rabani *et al*. [*Nature* **426** (2003) 271]) provide important insights into the coarsening (*i.e.* approach to equilibrium) of nanoparticle arrays. We conclude with a consideration of the near-term prospects for programmable matter.

1. Introduction

At the time of writing (Spring 2007), the field of complexity science is arguably rivalled only by nanoscience/nanotechnology when it comes to general expectation and hype. With this in mind, in this chapter we will attempt to consider the connections between these areas, focussing specifically on self-assembly, self-organisation, and non-linear dynamics in a prototypical nanostructured system: colloidal nanoparticle assemblies. Our aim is to provide a useful overview of

[1] The authors contributed equally to the work described in this chapter.

[2] Corresponding author. E-mail: philip.moriarty@nottingham.ac.uk, url: http://www.nottingham.ac.uk/physics/research/nano.

STUDIES IN MULTIDISCIPLINARITY
VOLUME 5 ISSN 1571-0831/DOI: 10.1016/S1571-0831(07)00001-9

pattern formation—both near to, and far from, thermodynamic equilibrium—in nanoparticle systems and to review current strategies to exploit self-organisation as a mechanism for pre-defined nanostructure fabrication. The emphasis is on the patterns formed in extremely thin ($\sim$ a few nm) films of nanoparticles on solid substrates. As this contribution necessarily represents a rather brief consideration of self-organised nanosystems, the particular subset of nanostructured materials we shall discuss will largely be informed by the authors' research interests and, thus (from a materials science perspective), will be relatively narrow in scope. Nevertheless, the system chosen for discussion (colloidal nanoparticle assemblies) exemplifies many key aspects of the physical properties and behaviour associated with the self-organisation of nanoscale units.

Perhaps 'complexity'—a nebulous term in many contexts—is most simply defined on the basis of Aristotle's observation in 150 BC that a system can be very much more than just the sum of its parts. That is, there is a particular "added value" arising from the interactions of the units (or "agents") comprising the ensemble. In terms of nanostructured systems, to illustrate many of the fundamental physical (and physicochemical) phenomena stemming from the interactions of large numbers of virtually identical units, we shall use what we consider the archetypal exemplar: nanoparticles dissolved in an organic solvent, forming a colloidal solution. Colloidal nanoparticles deposited from a solution onto solid surfaces form a rich variety of intricate patterns and the focus in the following discussion is to highlight morphological (and topological) parallels between nanostructured, microstructured, mesoscale, and macroscale systems formed via self-assembly and self-organisation.

To avoid potential confusion in later sections, we stress that we draw a distinction between the terms *self-assembly* and *self-organisation* where, throughout this chapter, the former is used to describe structures formed close-to-equilibrium whereas the latter refers to far-from-equilibrium dissipative processes involving energy/matter flow. Although this distinction is not always made in the literature, and in some cases the terms are used interchangeably, "self-organisation" has traditionally been reserved to describe processes occurring away from equilibrium. Perhaps the most important example, returning to the question of parallels with complex systems and complexity theory, is self-organised criticality. Although it is a moot point as to whether the systems we describe in the following sections can truly be described as complex systems (exhibiting emergent behaviour), there is no question that correlations in the spatial distribution of the nanoparticles occur on length scales far exceeding those associated with interparticle interactions. The development of correlations on mesoscopic length scales is, in our opinion, an important signature of a self-organised system; in self-assembly, interparticle interactions (perhaps mediated by the underlying surface) define the length scales of the observed patterns.

We note that other authors, most notably Whitesides and Grzybowski [1], have instead adopted somewhat different definitions. Whitesides and Grzybowski draw

a distinction between *static* and *dynamic* self-assembly, where they define the latter as arising only in dissipative systems. There is then an equivalence between the Whitesides and Grzybowski dynamic self-assembly process and self-organisation as described above. The colloidal nanoparticle assemblies described in the following sections could be seen to fall into yet a third class involving 'arrested' self-organisation (or, depending on the reader's preference, "arrested dynamic self-assembly"!). By "arrested", we mean that although the patterns may be defined by far-from-equilibrium processes such as convective flow, the system is strongly kinetically hindered at some point in its evolution so that even when the pattern-forming process is switched off, the associated structure is "frozen in".

2. Pattern Formation: Spanning the Nanoscopic to the Macroscopic

The striking array of patterns shown in Fig. 1.1 was created via a straight-forward experiment involving the deposition of a droplet of a nanoparticle/solvent solution onto a solid substrate (with subsequent evaporation of the solvent). In this case, the particles in question are alkylthiol-passivated Au nanoclusters of $\sim$2 nm diameter synthesised using the technique pioneered by Brust and co-workers [2]. Other types of nanoparticle, including, for example, CdSe [3] and PbSe [4], also produce a broad variety of complex patterns.

The physics underlying the appearance of the types of pattern seen in Fig. 1.1 and in similar systems is rather complex and can involve very many coexisting

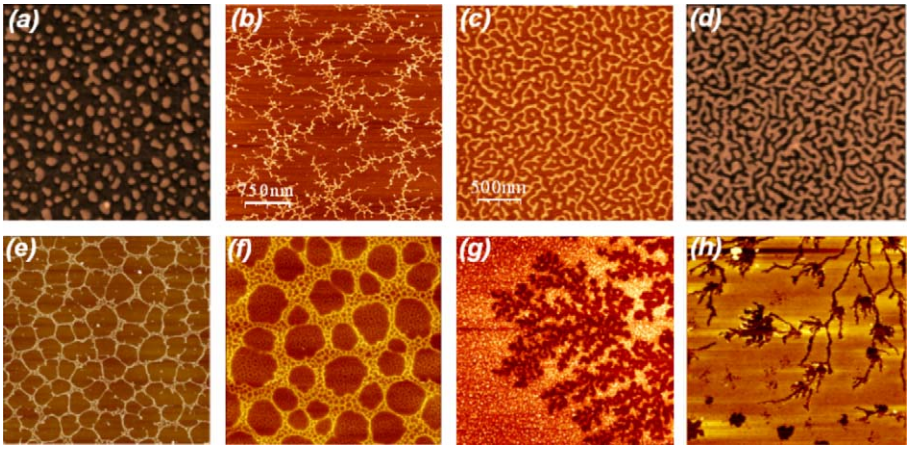

Fig. 1.1. A subset of the wide variety of patterns observed in colloidal nanoparticle assemblies formed via solvent evaporation. In each case tapping mode atomic force microscopy has been used to image the distribution of nanoparticles on a native oxide (SiO_2) covered Si(111) sample. The images shown in (a)–(e) and (h) are of single layers of nanoparticles whereas those in (f) and (g) are bilayer samples. For color, see Color Plate Section.

phenomena. These include (but are not limited to): the (de)wetting properties of the solvent–nanoparticle solution (on a given substrate); hydrodynamics (including the Marangoni effect [5]); phase transitions related to variations in solvent and nanoparticle density; instabilities in the solvent–nanoparticle fluid front; and nucleation/growth at the solid–liquid and/or liquid–air interface. Although some of these effects have previously been elucidated through experimentation and/or computer simulations [3–10], there remain very many open questions regarding the dynamics of pattern formation in colloidal nanoparticle assemblies.

The patterns shown in Fig. 1.1 range from isolated droplets (Fig. 1.1(a)) through dendritic/branched structures (Fig. 1.1(b)), worm-like and interconnected domains (Figs. 1.1(c) and (d)), and cellular networks (Figs. 1.1(e) and (f)), to relatively well-developed fractal morphologies (Figs. 1.1(g) and (h)). The interconnected and labyrinthine structures of Figs. 1.1(c) and (d) are, as shall be discussed below, strikingly similar to the self-organised patterns which form in binary fluid, polymer, and ferromagnetic systems. Importantly, Fig. 1.1 represents only a subset of the wide variety of patterns possible in colloidal nanoparticle systems: the parameter space associated with this—at first glance, rather simple—system is extremely wide. A significant point to realise is that many of the structures shown in Fig. 1.1 are formed far from equilibrium because the solvent (or the vast majority of the solvent) is rapidly driven off by spinning the sample at speeds of a few thousand rpm. As the nanoparticles are restricted from diffusing on the substrate in the absence of solvent [4,11], the system can be kinetically trapped very far away from its equilibrium state. In the limit of a perfectly wetting solvent–nanoparticle film, this equilibrium state is a single close-packed 'island' of nanoparticles covering a large surface area. Bigioni *et al.* [10] have, however, also shown that highly ordered assemblies comprising $\sim 10^8$ close-packed nanoparticles can be formed by seeding growth of the assembly at the *liquid–air* interface.

One might now enquire as to the "usefulness" of the various morphologies shown in Fig. 1.1 when it comes to developing novel nanostructured systems. Importantly, the majority of the different patterns shown in the figures are each associated with a particular length scale (or set of length scales). It is this presence of well-defined correlation lengths which makes the far-from-perfectly-ordered structures of Fig. 1.1 so interesting. First, the correlation lengths themselves (and other morphological/topological metrics) betray the influence of substantial long-ranged cross-talk between the elements of the system. These correlations in turn can represent a signature of a particular physical/physicochemical process. In the context of complex system dynamics, therefore, images of the type shown in Fig. 1.1 prompt questions related to the collective interaction of the nanoparticle units. The patterns shown have typical correlation lengths ranging from of order 100 nanometres to a few microns. This should be compared with the typical length scale associated with interparticle interactions which is of order a

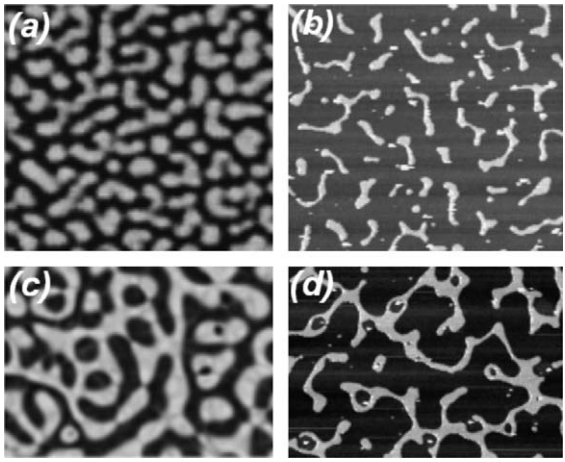

Fig. 1.2. A comparison of patterns formed in (a) phase-separating polymer and (c) binary fluid systems with those observed in colloidal nanoparticle assemblies ((c) and (d)). Figures (a) and (c) are reproduced from [13] and [14] respectively.

nanoparticle diameter (∼3 nm). Second, it is gaining control of this long-ranged collective behaviour that underpins much of the interest in pattern formation in far-from-equilibrium nanostructured systems.

Certain types of pattern are ubiquitous in nature and appear in a remarkably wide range of materials and across length scales differing by many orders of magnitude. (We refer the reader to a comprehensive and immensely readable account of pattern formation in nature written within the last few years by Ball [12].) To illustrate the ubiquity of the patterns which appear in nanostructured assemblies, we shall focus on the "worm-like", labyrinthine, and network structures shown in Figs. 1.1(c)–(f). Figure 1.2 places images of patterns formed in dewetting polymer films and phase separating binary fluids (Figs. 1.2(a) and (c) respectively) alongside atomic force micrographs of structures formed in nanoparticle assemblies (Figs. 1.2(b) and (d)). The qualitative similarity between Figs. 1.2(a) and (b) and between Figs. 1.2(c) and (d) is striking. Although close similarities in pattern formation of course do not *necessarily* arise from parallels in underlying physical/chemical behaviour, it is nevertheless important to note that polymer, binary fluid, and colloidal nanoparticle systems indeed share a number of common features. These include the influence of spinodal phase separation [3,4], nucleation and growth, and convective fluid flow on the evolution of the system. (We return to the question of the evolution/dynamics of pattern formation in Section 4 below.)

A structural motif which appears repeatedly in nanoparticle assemblies is the *cellular network* [7,8,15]. (*Cellular* in this case refers to the geometric cells (polygons) comprising the network and does not allude to biological cells.) We

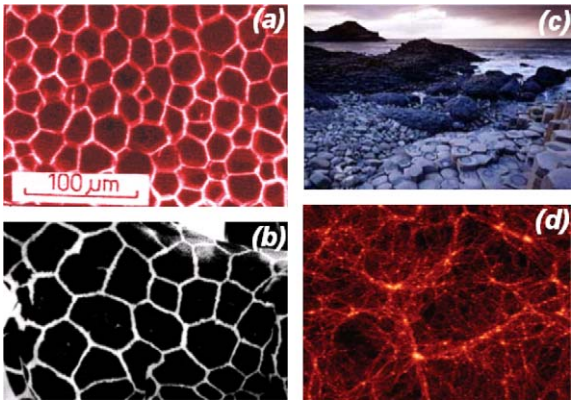

Fig. 1.3. Cellular networks in nature: (a) the microstructure of a cork [16]; (b) the cellular pattern formed on the hide of a giraffe; (c) the Giant's Causeway in Co. Antrim, Northern Ireland [17]; and (d) a frame taken from the Virgo Consortium Millennium simulation of the evolution of a structure in the Universe [18]. For color, see Color Plate Section.

have observed a cellular morphology ranging from relatively simple networks which are associated with a single correlation length (see, for example, Martin *et al*. [8]) to the rather more complex structures shown in Figs. 1.1(e) and (f) which comprise multi-level hierarchies of holes. Although the most widely recognised example is perhaps the foam formed by soap bubbles [15,19], a cellular structure of the type shown in Figs. 1.1(e) and (f) is ubiquitous in nature (as pointed out by Weaire and Rivier [15]). We show in Fig. 1.3 four examples of cellular networks ranging from the microstructure of a cork from a wine bottle to the large scale structure of the Universe. What is particularly intriguing about the morphology/topology of cellular networks is that it is possible, using the mathematics of statistical mechanics, to write down an equation of state for an ideal random cellular network which is analogous to the ideal gas law in classical thermodynamics [15,19]. Just as deviations from the ideal gas law betray the influence of new physics and chemistry, a statistical study of the structure of a cellular network (using Voronoi tessellations (see the following section) coupled with, for example, Lewis' law and the Aboav–Weaire law [15]) provides key insights into the relative importance of physics and chemistry *vs*. the mathematics of space filling in determining the structure of the system.

A particularly interesting example of multi-level network formation in nature (involving hierarchical distributions of holes/pores of different sizes) is found in the diverse set of complex microskeletons formed by the family of single-celled algae known as the diatoms. These fascinating structures were first described in detail by Haeckel in the late 19th century [20]. Diatoms—of which there are estimated to be $\sim 10^5$ distinct species—are capable of fabricating exquisitely microstructured silica shells which have, ever since the seminal work of

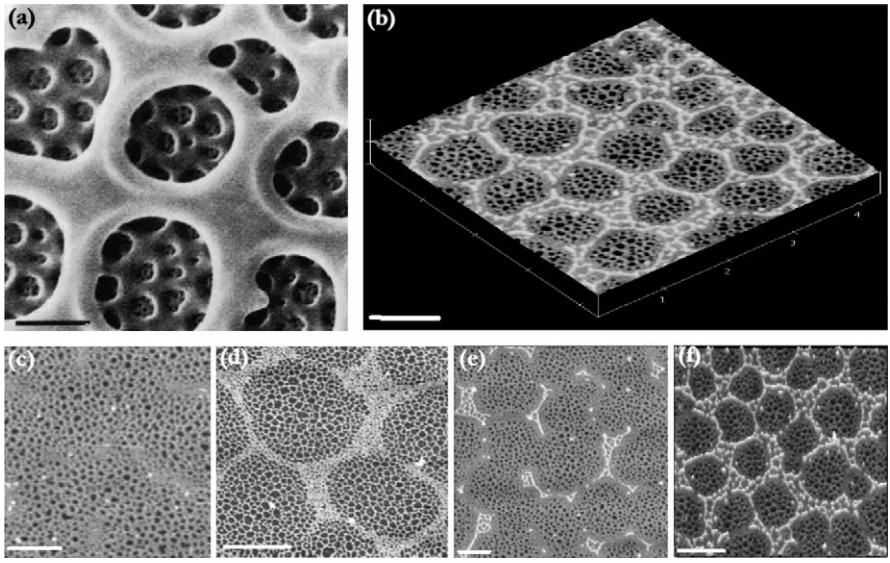

Fig. 1.4. Mimicking diatom microskeletons in colloidal (inorganic) nanoparticle assemblies. (a) A SEM image of the valve architecture of *Coscinodiscus wailesii* (taken from [26]). The scale bar in this image and all other images represents 1 μm. (b) A tapping mode AFM image of a 1.5 mg/ml solution of C5 thiol-passivated Au nanoparticles (2.2 nm mean diameter) spin cast (at 4 krpm) onto a native oxide terminated silicon substrate. (c)–(f) AFM images of nanoparticle array morphologies resulting from spin-casting 1.0, 1.1, 1.25, and 1.5 mg/ml solutions, respectively, onto silicon.

both Haeckel and D'Arcy Thompson [21], fascinated scientist and layman alike. While many aspects of pattern formation in diatom frustules remain to be elucidated [22–24], the potential for exploitation of this class of algae as a "nanofabricator" technology has garnered a remarkable amount of cross-disciplinary attention [25].

Although forming an impressively broad assortment of different patterns [20,23], a distinctive structural theme common to very many species of diatom is the *hierarchical* nature of the shell architecture. A striking example of this is shown in Fig. 1.4(a), a scanning electron microscope (SEM) image of the morphology of the valve of *Coscinodiscus wailesii* [26]. A similar type of hierarchical patterning is also observed in the (entirely abiotic) gold nanoparticle assembly shown in Fig. 1.4(b). The ability to pattern matter via self-assembly/self-organisation across a range of different length scales, as exemplified by Figs. 1.4(a) and (b), is an increasingly important goal in nanoscience [27] and a substantial amount of the intense recent interest in the potential nanotech applications of diatoms stems from this morphological characteristic. (Moreover, ground-breaking efforts by Oliver *et al*. [22] have resulted in the fabrication of artificial diatom microskeleton forms via advanced inorganic morphosynthesis.)

The nanoparticle assembly of Fig. 1.4(b) clearly comprises cellular networks—"foams"—having two very distinct length scales. Of particular significance to multiple length scale patterning, a short wavelength network formed in the first monolayer of particles is embedded within a larger cellular structure in the second layer, mimicking the hierarchical structuring (at the micron and sub-micron levels) of the diatom frustules shown in Fig. 1.4(a). We suggest that two distinct processes with well-defined correlation lengths—namely Marangoni convection [6] and the coalescence of randomly nucleated holes in the solvent–nanoparticle film [8]—drive the generation of the micron and sub-micron scale nanoparticle foams observed in Fig. 1.4(b). (As initially shown by Ge and Brus [3] and confirmed in recent simulations by Rabani *et al*. [4], spinodal decomposition can also play a role in forming spatially correlated nanoparticle patterns.) Although in previous works [7,8] we have discussed the ability of far-from-equilibrium assembly to generate nanostructured cellular networks, the diatom-like, 'foam within foam' patterning observed in Fig. 1.4(b) is an entirely new and unexpected nanoparticle array morphology. Its origins may be ascertained from an examination of Figs. 1.4(c)–(f).

Figures 1.4(c)–(f) show the nanoparticle array morphology arising from spin-coating progressively more concentrated nanoparticle solutions onto the silicon substrate. Note the absence of hierarchical patterning in Fig. 1.4(c) and its gradual emergence as the solution concentration is gradually increased. The most plausible origin of the longer length scale network present in Figs. 1.4(d)–(f) is the Marangoni effect: a convective flow driven by the temperature gradient imposed due to the evaporation of the volatile solvent (in this case, toluene) [6,28]. In Fig. 1.4(d), a polygonal network (whose cells are spaced by approximately 1 micron) of densely packed nanocrystals in the first monolayer is observed and, as shown in Figs. 1.4(e) and (f), acts as a template for the adsorption of the second layer of nanoparticles (Figs. 1.1(e) and (f)). We are confident that there is a particular scope to program both the degree of network order and the associated correlation lengths (via, for example, the establishment and control of spatially well-defined temperature fields during solvent evaporation).

3. Quantifying Morphology and Topology

Although qualitatively striking, it is obviously important to consider metrics that might be used to classify *quantitatively* the morphology and topology of the various nanostructured patterns shown in the previous sections. Not only is this necessary from the perspective of determining, for example, the connectivity and correlations within a given structure but quantitative metrics can be applied to ascertain what parallels might exist between apparently disparate systems. Although Fourier (and wavelet) analysis can be used to determine correlation lengths and

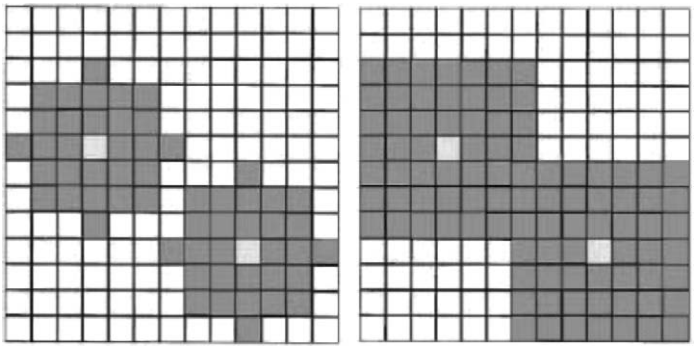

Fig. 1.5. The 'grain growth' approach to image analysis using Minkowski measures [30]. The decoration of germs (light grey) with grains (dark grey) that are discrete approximations to circles (left) and squares (right).

degrees of orientational order, sophisticated complementary methods such as statistical crystallography [15] and Minkowski morphometry [30] are increasingly being used to characterise the morphology and topology of nanostructured systems.

We have previously [7,8] used Voronoi tessellations [15] to elucidate the degree of spatial correlation (*i.e.* deviations from Poisson statistics) in nanoparticle assemblies. Mecke *et al.* [29] pioneered the use of Minkowski functionals in the analysis of spatial correlations in dewetting polymer films. In 2D, the Minkowski functionals [30] are reduced to three relatively straight-forward geometric measures: the total covered area, the total perimeter length, and the Euler characteristic. This latter measure effectively accounts for the number of interconnected regions in an image [30] and is of obvious significance if the connectivity of a nanostructured system is of interest (in, for example, electron transport via percolation).

From an image where the centres of mass of the morphological features may be readily identified, Minkowski analysis may be applied using the method described in the review article by de Raedt *et al.* [30] and schematically shown in Fig. 1.5. From each initial "germ" (of edge length $r = 1$) representing the centre of mass of a feature in the original image (*e.g.* a hole in an otherwise continuous film or an island of material on a substrate), a square "grain" of edge length $2r+1$ is grown and the Minkowski measures are calculated for each grain size or, more correctly, as a function of the normalised quantity $x = r/L$ where L is the mean germ separation. Different spatial distributions of the germs will produce marked differences in plots of the Minkowski measures (perimeter, area, or Euler characteristic) against x.

A number of groups have discussed the application of Minkowski measures to the analysis of structure formation in polymer thin films [29,31,32]. Cer-

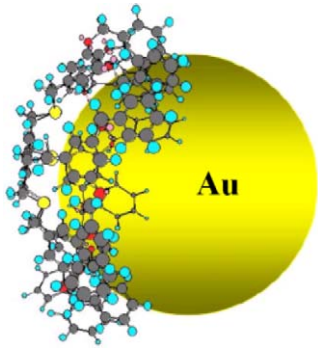

Fig. 1.6. A simple schematic illustration of an Au nanoparticle terminated by a 3,5-Bis(benzyloxy)benzylbromide S6G1 dendrimer. For color, see Color Plate Section.

tain classes of pattern, however, specifically those associated with the nucleation and growth of holes or islands, give rise to effectively *system-independent* Minkowski characteristics. That is, despite having dramatically different materials characteristics, the same types of spatial correlations are seen in many systems. What is the origin of these similarities? To attempt to address this question we will consider a nanoparticle system which is markedly different from that discussed thus far. In Fig. 1.6 we show a schematic diagram of a gold nanoparticle where the surface-terminating species is not a simple thiol molecule but a 3,5-Bis(benzyloxy)benzylbromide S6G1 *dendrimer* [33,34]—a complex branched polymer. Dendrimers [35] are increasingly used as stabilising agents for nanoparticle surfaces as they have a well-defined molecular weight, size, and structure and they can encapsulate both organic and inorganic hosts. We show in the following that despite these significant differences in nanoparticle size and structure, morphological measures based on Voronoi tessellations and Minkowski functionals show that there are striking parallels in the structure of assemblies of thiol- and dendrimer-terminated nanoparticles. Indeed, these parallels extend to entirely unrelated materials systems such as polymers [8] and small organometallic molecules [36].

Figure 1.7(a) shows the adsorbed "film" formed by S6G1-terminated Au nanoparticles following spin-coating of a colloidal solution of the particles on a silicon substrate. The dendrimer-stabilised nanoparticles aggregate to form globular structures with heights and diameters of order 50 and 250 nm respectively. In common with previous AFM measurements of spin-coated dendrimer films [37], we observe a relatively high density of 'droplets'. What is intriguing, however, is that even from an initial qualitative appraisal of the images, the positions of the dendrimer-functionalised nanoparticle droplets appear to be spatially correlated to some degree (*i.e.* there are strong deviations from a Poisson-distributed point set). (This is true also of the images reported by Sano *et al.* [37].) To put our

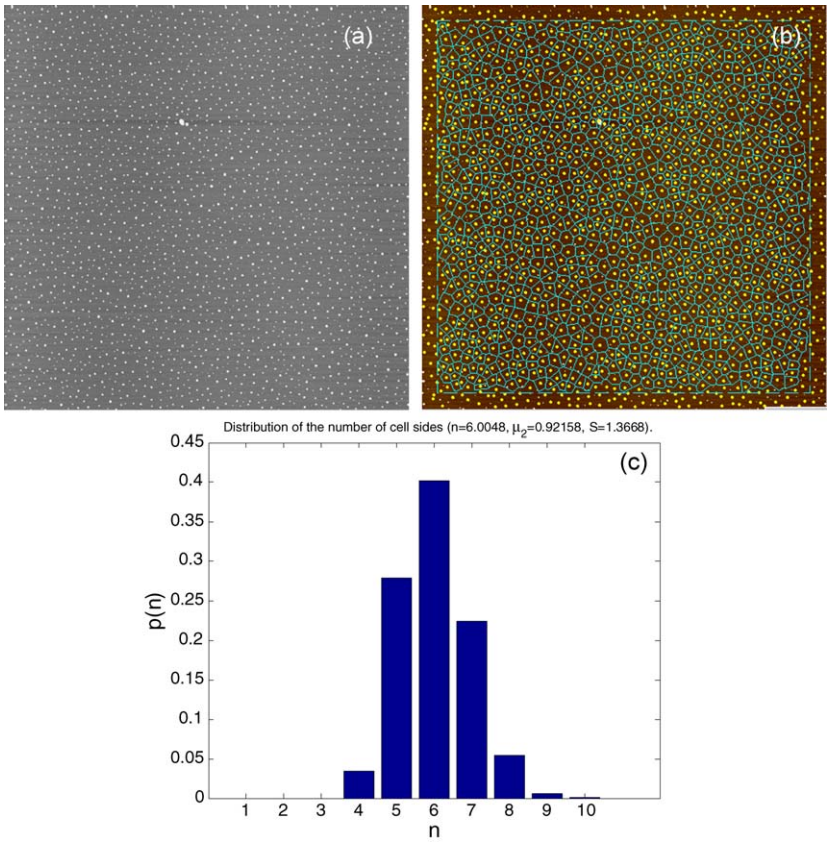

Fig. 1.7. (a) A tapping mode atomic force microscope (AFM) image (40×40 μm^2) of the film morphology formed by spin-coating a solution of dendrimer-functionalised Au nanoparticles in toluene onto a native oxide-terminated Si(111) substrate. Note that the nanoparticles aggregate to form droplets with a relatively narrow size distribution and with an apparent ordering in their spatial distribution. (b) A Voronoi tessellation constructed from the centres of the droplets shown in (a). (c) A histogram of the probability, $p(n)$, of finding an n-sided cell. For color, see Color Plate Section.

discussion on a firmer quantitative footing, we have carried out Voronoi tessellation and Minkowski functional analyses for the dendrimer–nanoparticle aggregate distributions (see Figs. 1.7(b) and 1.8).

A Voronoi tessellation is the statistical crystallography analog of the Wigner–Seitz unit cell used extensively in conventional crystallography and condensed matter science. Briefly, the tessellation shown in Fig. 1.7(b) was constructed by: (i) identifying the centre of mass of each of the nanoparticle droplets shown in Fig. 1.7(a), (ii) connecting each centre of mass to its nearest neighbours, and (iii) finding the perpendicular bisectors of those connecting lines. This produces, for each droplet, a Voronoi cell (a polygon) which represents the smallest surface

area associated with that droplet. The subsequent analysis of the distribution of polygon *sidedness* (*i.e.* the number of polygon sides), area, and perimeter length can yield substantial insights into the physics underlying the formation of a particular surface morphology. From the distribution of polygon sidedness shown in Fig. 1.7(b), it is straightforward to calculate a 'tessellation entropy' (a quantity that is obviously very much distinct from the overall thermodynamic entropy of the system) which is defined in an analogous fashion to the conventional statistical mechanics form: $S = -\sum p_n \ln p_n$, where p_n is the probability associated with finding an n-sided polygon. For a Poisson point set, the tessellation entropy is $\sim$1.75. For the image shown in Fig. 1.7(b), and in common with a number of other nanostructured systems [7,8], we find an entropy of $\sim$1.4 (to two significant figures). That the value of S for the distribution of aggregates shown in Fig. 1.7(a) falls substantially below that expected for a Poisson distribution is indicative of the presence of spatial correlations in the nanoparticle arrangement. Moreover, it is intriguing that a value of $S = 1.40(\pm 0.05)$ is associated with a rather broad range of nanostructured thin films: could this be indicative of a common origin for the deviation from Poisson statistics.

To address this question, we have calculated the variation of the Minkowski measures with 'grain' size, as described above. The deviation from a Poisson point set is also apparent from the Minkowski measure analysis. We show in Fig. 1.8 the variation of the Euler characteristic, χ, as a function of x for the distribution of nanoparticle aggregates shown in Fig. 1.7(a). (Note that although in general it is important to consider variations in all three Minkowski measures, we focus here on the Euler characteristic as a representative example of the analysis technique.) Figure 1.8(a) is a comparison of the variation in χ for the image shown in Fig. 1.7(a) with the variation expected for a Poisson point set. The difference between these quantities is shown in Fig. 1.8(b) where the deviation from Poisson statistics is clear, in agreement with the Voronoi tessellation analysis of Fig. 1.7. The Minkowski measures, however, provide substantially more insight into the morphology and topology of a system. Perhaps more importantly, the Euler characteristics shown in Fig. 1.8 overlap almost perfectly with those measured in very different systems including dewetting organometallic thin films [36] and thiol-passivated Au nanoparticles [8].

How does this similarity in morphological characteristics arise and, in particular, why are strong deviations from Poisson statistics observed in each of these systems? Although phenomena such as spinodal decomposition/dewetting or Marangoni convection are inherently associated with well-defined correlation lengths, in the systems discussed above and, in particular, that shown in Fig. 1.7, we have proposed [8] that the deviations from spatially uncorrelated morphological features arise simply from coalescence events which wipe out the clustering that is the signature of a Poisson distribution of points. Brinkmann *et al.* [38,39] have previously observed similar strong mesoscopic correlations in the positions

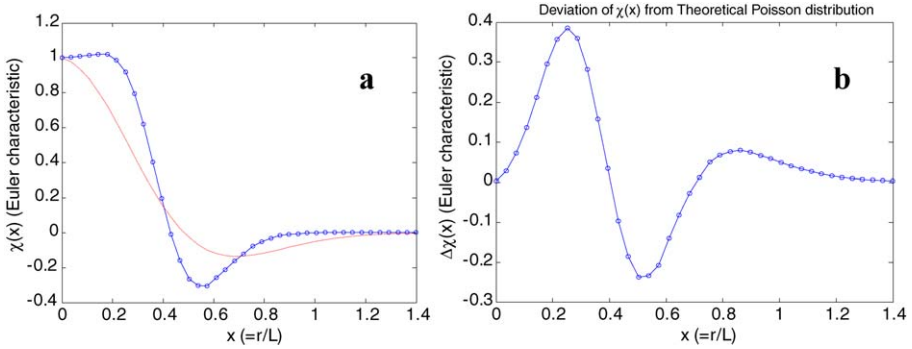

Fig. 1.8. (a) The variation of the Euler characteristic as a function of normalised grain size (see text for a discussion) for a point set derived from the centres of the droplets shown in Fig. 1.7(a). The graph in (b) shows the deviation of the Euler characteristic from that expected for a Poisson (spatially uncorrelated) distribution of points. For color, see Color Plate Section.

of islands of organic molecules deposited by *vacuum sublimation* onto silicon substrates. They attribute the emergence of a cut-off distance in the distribution of nearest neighbour separations to the merging of neighbouring aggregates either via direct coalescence (touching) of two islands or via a ripening phenomenon involving overlapping island diffusion fields. Regardless of the coalescence mechanism, it is from some perspectives remarkable that an undirected assembly process (occurring on a homogeneous substrate) can give rise to such striking spatial correlations in disparate systems (colloidal nanoparticles *vs*. vacuum-deposited organic molecules). An open question relates to the degree to which the correlations can be tuned or programmed—an issue of obvious importance for self-organised nanostructured systems.

4. Evolving to Equilibrium

Returning to a consideration of the thiol-passivated nanoparticle patterns shown in Fig. 1.1, Rabani *et al*. [4] have put forward an Ising model description of drying-mediated pattern formation in nanoparticle–solvent films where the Hamiltonian of Eq. (1) is used within a Monte Carlo algorithm to model the system dynamics.

$$H = -\epsilon_l \sum_{ij} l_i l_j - \epsilon_n \sum_{ij} n_i n_j - \epsilon_n l \sum_{ij} n_i l_j - \mu \sum_i l_i. \qquad (1)$$

This model reproduces many (though certainly not all—see below) of the types of patterns we [7,8] and others [3] observe experimentally and has also been shown to yield good agreement with experimental data on the dynamics of nanoparticle aggregate (*i.e.* cluster) growth [4]. Equation (1) comprises (from left

to right) terms describing nanoparticle–nanoparticle, nanoparticle–solvent, and solvent–solvent interactions, with the final term related to the chemical potential of the solvent (which accounts for the solvent evaporation rate/vapour pressure).

Changes in the value of the total (global) energy of the system (represented by the Hamiltonian in Eq. (1)) are used to assign probabilities (via a Boltzmann factor, $\exp(-\frac{\Delta H}{kT})$) for a number of processes to occur (*i.e.* the standard Metropolis algorithm Monte Carlo strategy [40] is implemented). In the nanoparticle–solvent system of interest here, the dynamic processes are limited by Rabani *et al*. [4] to solvent evaporation/condensation and nanoparticle hopping on the substrate. Importantly, nanoparticles do not diffuse on dry substrate: the model restricts nanoparticle hopping into sites which are occupied with the solvent. As highlighted by Rabani *et al*., it is this coupling between the solvent and nanoparticle dynamics which gives rise to much of the interesting behaviour of the system. For certain classes of pattern, the Rabani *et al*. approach produces remarkable agreement with experiment [4,8].

The process by which a far-from-equilibrium system approaches its equilibrium state is known as *coarsening* or *ripening*. Just as the snapshots of patterns shown in the figures thus far (where each image shows the system at a particular point in time) exhibit striking system-independent morphologies, coarsening is a ubiquitous phenomenon which displays a key universal feature: a temporal self-similarity of the sample morphology. (For an excellent review of coarsening in 2D systems, see Zinke-Allmang [41].) The self-similar nature of the coarsening process means that the evolution of the system towards equilibrium needs only one parameter—the fundamental length scale—for its description. This length scale, r, follows a power-law dependence on time, *i.e.* $r \sim t^{\gamma}$, where γ is the growth exponent. Different diffusion mechanisms (which underlie the coarsening process) give rise to different values of γ (although it is important to note that knowledge of γ alone is not always sufficient to correctly characterise the coarsening mechanism). Perhaps of most relevance to the central theme of this book, the self-similarity inherent in coarsening systems enables a pattern initially present at the nanometre scale to be preserved and "expanded", in principle, up to micron (or larger) length scales.

In recent experiments we have observed a striking coarsening of nanoparticle assemblies driven by a scanning probe [42]. In this coerced coarsening phenomenon, the degree of "pattern expansion" is tunable simply by interrupting the scan process at a pre-defined time. As the work on probe-induced coarsening is detailed elsewhere [42], we shall instead focus here on an analysis of the evolution of a nanoparticle assembly (formed in the spinodal regime of solvent evaporation) using the Monte Carlo simulation described above. Figure 1.9 shows three snapshots from a simulation of the evolution of a "spinodal" assembly. It is clear that, as time progresses, while the average size and spacing of the domains increase, the general form of the pattern does not change. This is clear from an analysis

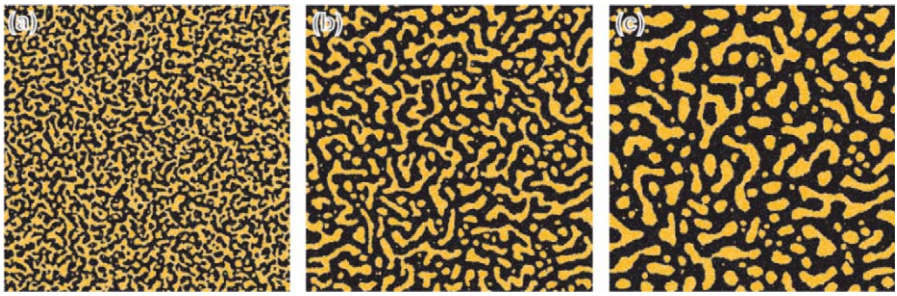

Fig. 1.9. Three frames showing coarsening of a nanoparticle assembly formed by solvent evaporation in the spinodal regime. (Simulation parameters: 1008 × 1008 pixel system with $k_{\mathrm{B}}T = \epsilon_l/2$, MR = 30, and a nanoparticle coverage of 30%.) (a) After 39 Monte Carlo steps, the majority of the solvent has already evaporated leaving only a thin wetting layer around the domains; (b) after 299 MC steps, a visibly increased length scale is present, and (c) after 999 MC steps where the length scale has clearly increased further. For color, see Color Plate Section.

of the radially averaged Fourier transforms of the images (not shown). With appropriate scaling so that the magnitude of the transform is plotted not against q (where q represents wavevector) but against $q/q_{\max}$ (where $q_{\max}$ is the value of q at which the Fourier transform peaks, representing the "signature" length scale of the system), the Fourier transforms collapse onto a time-independent master curve [42,47].

As the position of the peak in the radially averaged Fourier transform ($q_{\max}$) represents the correlation length of the coarsening system at a given point in time, by plotting $q_{\max}$ versus MC step number (*i.e.* time) on a log–log scale, it is possible to extract the value of the growth exponent, γ. Rabani *et al*. [4] have shown that for nanoparticle assemblies comprising ensembles of isolated islands, the mean island radius scales so that $\gamma = 0.25$. An interesting question is whether the interconnected morphology of the assemblies shown in Fig. 1.9 might produce a different scaling exponent (*i.e.* are different diffusion pathways active?). Both experimental data [42] and the results of MC simulations (see Fig. 1.10(a)) indicate that the exponent of 0.25 is preserved in the spinodal regime. Figure 1.10(a) is a log–log plot of $q_{\max}$ *vs*. number of MC steps and it is clear that the slope of the graph asymptotically approaches -0.25 (the negative sign arises because in this case we have plotted wavevector rather than wavelength against time). We have recently verified that the 0.25 exponent derived from Fig. 1.10(a) for a relatively short simulation time does not change for simulation times up to a few hundred thousand MC steps. That is, in Fig. 1.10(a) the system has reached the appropriate scaling regime.

We have also examined the evolution of the various Minkowski measures for the nanoparticle assembly shown in Fig. 1.9. Intuitively, the boundary length, U, of this structure will decrease over time. This can be used as a measure of

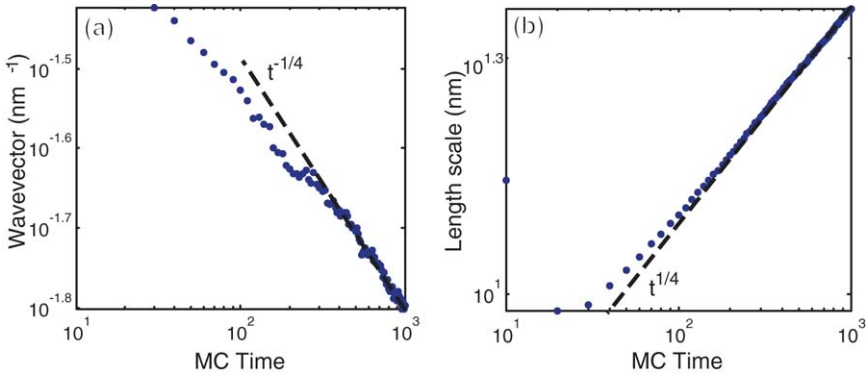

Fig. 1.10. Analysis of the scaling regime in the evolution of a 'spinodal' nanoparticle assembly showing (a) the evolution of the peak in the 2D FFT, and (b) the evolution of the length scale $L = A_{\text{total}}/U$ of the pattern (where U is the total perimeter length—a 2D Minkowski measure). Both reveal an approach to an exponent of $1/4$. For color, see Color Plate Section.

the length scale of the pattern. We can define a length scale, $L = A_{\text{total}}/U$, where A_{total} is the total area of the simulation grid. L is then a measure of the mean size of features in the image and, as shown in Fig. 1.10(b), this quantity follows the same growth law ($\gamma = 0.25$) as the peak in the Fourier transform. More importantly, Minkowski measures can be used to demonstrate that despite an increasing length scale, the pattern retains the same *morphology*. If the Euler characteristic scales in the same manner as the perimeter, then the pattern can be said to be morphologically stable. The value of χ/U should tend to a constant, and the value of $\frac{\mathrm{d}(\chi/U)}{\mathrm{d}t}$ should therefore tend to zero. This is indeed the case: such a plot drops to within 10^{-4} of zero after 100 MC steps, and after 400 MC steps there is an even clustering around zero.

Finally, despite its ability to accurately (and impressively) reproduce many of the patterns observed experimentally in colloidal nanoparticle assemblies (and their associated dynamics), there are a number of very important limitations of the Monte Carlo model described above. Many of the key limitations stem from the fact that only solvent evaporation or condensation is incorporated in the algorithm—*there is no flow of solvent possible*. In other words, although the nanoparticles hop on the substrate, the solvent molecules do not diffuse from site to site.

This restriction in turn means that the effects of convective solvent dewetting cannot be reproduced in the Monte Carlo code. To build in convective dewetting processes requires not only a consideration of solvent diffusion but the modelling of a solvent film which can have local 2D or 3D character in different regions of the surface. (We are currently developing code which incorporates dewetting phenomena of this type [43].) Important additional effects not built into the model—and pointed out by Rabani *et al*. [4] in the conclusions of their paper—are hydro-

dynamics driven by Marangoni convection [6,7] and front instabilities (which the results of our recent experiments [44] suggest are strongly mediated by solvent dewetting). These front instabilities give rise to structures very reminiscent of the "viscous fingering" patterns observed in a range of systems including mixtures of viscous and inviscid fluids and solidification from a melt. What is of particular importance is that each of these effects can be, in essence, "programmed" by varying the substrate chemistry, opening new avenues of research in *directed* assembly of nanostructured systems [42].

5. Conclusions

Colloidal nanoparticle assemblies represent a fascinating archetype for the study of self-assembly, self-organisation, and pattern formation in nanostructured systems. Many complex and intricate patterns result from a rather simple experiment where droplets of colloidal solution are deposited or spun onto solid substrates. Despite the simplicity of the experiment, a variety of complex physicochemical effects give rise to intricate (but generally spatially correlated) patterns ranging from isolated nanoscale droplets through labyrinthine structures to fractal branches. In this chapter some of the phenomena underlying the origin and evolution of patterns in nanoparticle assemblies have been described but in many ways we (*i.e.* the nanoscience research community) have barely "scratched the surface" both in terms of our understanding of self-assembly and, of key importance, in developing protocols to reliably tune or, more excitingly, *program* the assembly/organisation process.

Pioneering steps in controlling the assembly of nanoparticle arrays have been made by a number of groups (including Refs. [3,4,10,45,46] amongst others) but it is clear that even in arguably the most basic colloidal nanoparticle system (thiol-passivated Au clusters) there is a very wide parameter space associated with pattern formation. When one considers the broad variety of functional groups that can be added to either the nanoparticle or the substrate surface, the parameter space associated with pattern formation becomes not just wide but vast! As such, we can expect to continue to see (for quite some time) a wealth of exciting fundamental and applied science on self-assembly and self-organisation in colloidal nanoparticle arrays.

Arguably, however, the most exciting element of the self-assembly/self-organisation processes described above lies in their potential to lead to *programmable* assembly of matter. Software compilation of matter from individual molecules forms the core of the molecular manufacturing concept pioneered by K. Eric Drexler in his book *Nanosystems* [48]. Although molecular manufacturing is an extremely controversial subject within the nanoscience community (see, for example, [49–52]), at its core lies an important and demonstrably valid idea: computer-controlled single molecule chemistry. In the Drexler scheme, the

position of each atom in a macroscopic structure is completely defined and the structure is assembled via entirely deterministic molecular trajectories.

An alternative approach to the realisation of programmable matter is to tune the pattern-forming processes described above. This could be achieved via a variety of physicochemical parameters including electric and magnetic field strengths (and/or frequencies, phases, *etc*.), pH differences, and optical wavefields. Of course, the exploitation of one or more of these parameters in directed self-organisation necessitates a careful consideration of the thermodynamic and kinetic constraints on a particular system and thus, although a number of groups are currently pursuing research programmes involving directed assembly, progress is relatively slow. Nevertheless, a number of approaches—including the use of genetic algorithms to tune a nanostructured system towards a particular type of non-equilibrium state—appear viable and we are confident that in the next decade important advances will be made in the area perhaps best described as "matter compilation".

Acknowledgements

The authors gratefully acknowledge funding from the European Commission under Sixth Framework contract HMT-RTN-200450728 (the *PATTERNS* Marie Curie Research Training Network (RTN)). This work was also supported by a Fifth Framework RTN, *Supramolecular Self-Assembly of Interfacial Nanostructures* (*SUSANA*) (HPRN-CT-2002-00185) and by the UK Engineering & Physical Sciences Research Council (EPSRC). We thank members of the *PATTERNS* network (in particular, Uwe Thiele, Ulli Steiner, Mathias Brust, and Bosa Tadic) for extremely helpful and enlightening discussions on pattern formation in thin film and nanostructured systems.

References

[1] George M. Whitesides, Bartosz Grzybowski, *Science* **295** (2002) 2418.
[2] M. Brust, M. Walker, D. Bethell, D.J. Schiffrin, R. Whyman, *J. Chem. Soc. Chem. Comm.* **1994** (1994) 801.
[3] G. Ge, L. Brus, *J. Phys. Chem. B* **104** (2000) 9573.
[4] E. Rabani, D.R. Reichman, P.L. Geissler, L.E. Brus, *Nature* **426** (2003) 271.
[5] M.P. Pileni, *J. Phys. Chem. B* **105** (2001) 3358.
[6] M. Maillard, L. Motte, M.P. Pileni, *Adv. Mat.* **13** (2001) 200.
[7] P. Moriarty, M.D.R. Taylor, M. Brust, *Phys. Rev. Lett.* **89** (2002) 248303.
[8] C.P. Martin, M.O. Blunt, P. Moriarty, *Nano Lett.* **4** (2004) 2389.
[9] X.M. Lin, H.M. Jaeger, C.M. Sorensen, K.J. Klabunde, *J. Phys. Chem. B* **105** (2001) 3353.
[10] T.P. Bigioni, X.M. Lin, T.T. Nguyen, E.I. Corwin, T.A. Witten, H.M. Jaeger, *Nature Materials* **5** (2006) 265.
[11] J.N. O'Shea, M.A. Phillips, M.D.R. Taylor, P. Moriarty, M. Brust, V.R. Dhanak, *Appl. Phys. Lett.* **81** (2002) 5039.

[12] Philip Ball, *The Self-Made Tapestry: Pattern Formation in Nature*, Oxford University Press, 2001.
[13] K. Fukunaga, H. Elbs, G. Krausch, *Langmuir* **16** (2000) 3474.
[14] H. Tanaka, T. Araki, *Phys. Rev. Lett.* **81** (1998) 389.
[15] D. Weaire, N. Rivier, *Contemp. Phys.* **25** (1984) 59.
[16] Sidney Perkowitz, *Universal Foam*, Walker & Co., New York, 2000.
[17] Image taken from The National Trust website: www.nationaltrust.org.uk.
[18] www.virgo.dur.ac.uk.
[19] N. Rivier, *Philos. Mag. B* **52** (1985) 795.
[20] E. Haeckel, *Challenger Monograph* (1887).
[21] D. Thompson, *On Growth and Form*, Cambridge University Press, Cambridge, 1917.
[22] O. Oliver, et al., *Nature* **378** (1995) 47.
[23] G.A. Ozin, *Acc. Chem. Res.* **30** (1997) 17.
[24] M. Sumper, *Science* **295** (2002) 2430.
[25] *Journal of Nanoscience and Nanotechnology* (January 2005) devoted entirely to diatom nanotechnology.
[26] A.-M.M. Schmid, B.E. Volcani, *J. Phycol.* **19** (1983) 387.
[27] M.D. Morariu, N.E. Voicu, E. Schaffer, Z.Q. Lin, T.P. Russell, U. Steiner, *Nature Materials* **2** (2003) 48.
[28] H. Bénard, *Rev. Gen. Sci. Pures Appl. Bull.* **11** (1900) 1261.
[29] K. Jacobs, S. Herminghaus, K.R. Mecke, *Langmuir* **14** (1998) 965.
[30] K. Michielsen, H. De Raedt, *Phys. Rep.* **347** (2001) 461.
[31] J. Becker, G. Grun, R. Seemann, H. Mantz, K. Jacobs, K.R. Mecke, R. Blossey, *Nature Materials* **2** (2003) 59.
[32] J. Rysz, *Polymer* **46** (2005) 977.
[33] S.W. Chen, R.W. Murray, *Langmuir* **15** (1999) 682.
[34] A. D'Aléo, R.M. Williams, F. Osswald, P. Edamana, U. Hahn, J. van Heyst, F.D. Tichelaar, F. Vögtle, L. De Cola, *Adv. Funct. Mat.* **14** (2004) 1167.
[35] F. Vögtle, S. Gestermann, R. Hesse, H. Schwierz, B. Windisch, *Prof. Poly. Sci.* **25** (2000) 987.
[36] F. Frehill, K.H.G. Schulte, C.P. Martin, L. Wang, S. Patel, J.A. Purton, J.G. Vos, P. Moriarty, *Langmuir* **20** (2004) 6421.
[37] M. Sano, J. Okamura, A. Ikeda, S. Shinkai, *Langmuir* **17** (2001) 1807.
[38] M. Brinkmann, F. Biscarini, C. Taliani, I. Aiello, M. Ghedini, *Phys. Rev. B* **61** (2000) R16339.
[39] M. Brinkmann, S. Graff, F. Biscarini, *Phys. Rev. B* **66** (2002) 165430.
[40] G. Casella, C.P. Robert, *Monte Carlo Statistical Methods*, Springer-Verlag, New York, 2004.
[41] M. Zinke-Allmang, *Thin Solid Films* **346** (1999) 1.
[42] M. Blunt, et al., *Nature Nanotech.* **2** (2007) 167.
[43] C.P. Martin, et al., unpublished.
[44] E. Vaujour, et al., unpublished.
[45] R.P. Andres, J.D. Bielefeld, J.I. Henderson, D.B. Janes, V.R. Kolagunta, C.P.V. Kubiak, W.J. Mahoney, R.G. Osifchin, *Science* **273** (1996) 1690.
[46] C.J. Kiely, J. Fink, M. Brust, D. Bethell, D.J. Schiffrin, *Nature* **396** (1998) 444.
[47] H.-J. Ernst, F. Fabre, J. Lapujoulade, *Phys. Rev. Lett.* **69** (1992) 458.
[48] K. Eric Drexler, *Nanosystems: Molecular Machinery, Manufacturing, and Computation*, Wiley Interscience, Chichester, 1992.
[49] K. Eric Drexler, R.E. Smalley, *Chem. Engng. News* **81** (2003) 37.
[50] http://www.softmachines.org/wordpress/index.php?p=70.
[51] P. Moriarty, *Nanotechnology Perceptions* **1** (2005) 115.
[52] http://video.google.com/videoplay?docid=-6086023528639836493.